ORIGINAL PAPER

Trapped Field in Superconductors with Perforations

A. N. Maksimova[1] · V. A. Kashurnikov[1] · A. N. Moroz[1] · D. M. Gokhfeld[2,3]

Abstract

The Monte Carlo method has been used to calculate the trapped magnetic field in superconducting plates with holes. The mechanism of flux pinning on the holes is implemented with special subprocesses added to the algorithm: vortex capture and emission, both occurring on the hole boundaries. Secondary peaks related to the holes emerge on the calculated profiles of the trapped magnetic field. It has been found that these peaks disappear in plates with sufficiently strong pinning or when the computational mesh is coarse (the case corresponding to a low resolution of probes in experiments). The dependence of the trapped field on the hole radius has been analyzed.

Keywords Trapped flux · Vortex pinning · Monte Carlo · Trapped field magnet · HTS foam

1 Introduction

The nondissipative mode of current flow in a high-temperature superconductor (HTS) at a given external field H and temperature T is limited by the value of the critical current density j_c. High critical currents can be achieved in HTSs by introducing additional defects acting as pinning centers for the magnetic flux.

The typical methods of creating pinning centers include the introduction of nanoparticles [1–3] or various impurities [4–6] in HTS and irradiation [7, 8]. Also, creating artificial perforations is an advanced method of improving the transport characteristics of superconductors [9–11]. In work [9], through-holes were formed in a superconducting layer by means of femto- and picosecond laser pulses. Such defects have a diameter of about several micrometers and their size is much greater than the size of a vortex. However, collective pinning of Abrikosov vortices can be effectively implemented on the boundary of the superconducting and non-superconducting regions.

To define the optimal conditions for flux pinning on artificial holes, investigations of a large number of samples with different configurations and sizes of holes are required. For this task, numerical modeling being a very powerful method is convenient. It provides an opportunity of varying the size, configuration, and the number of different structural inhomogeneities of the sample in wide ranges and allows one to separate their influence on j_c from that of numerous other factors. Likewise, simulations allow one to analyze the differences in performance of various defects and vary their effective depth α (the characteristic energy of vortex-defect interaction) and concentration. Substantial attempts to determine the optimal configuration of holes by means of computations were made in paper [12], where the Bean model was used to calculate the magnetization and current distributions. The configurations providing maximum trapped flux were also calculated. In work [13], the finite element method was used for similar purposes.

In this paper, we consider the effect of perforations in an HTS on the trapped field by means of the Monte Carlo (MC) method. Previously, a method based on the MC algorithm capable of modeling the vortex lattice in a superconductor was developed. In works [14–16], the dynamics of the Abrikosov vortex system were simulated in an HTS with defects in the form of holes (antidots) and the resulting critical current was calculated. A qualitative explanation of the nonmonotonic dependence of the critical current on the hole size (observed in real experiments) was proposed. The calculations showed that the drop in j_c with the increasing antidot

✉ D. M. Gokhfeld
gokhfeld@iph.krasn.ru

1 National Research Nuclear University MEPhI,
Moscow 115409, Russia

2 Kirensky Institute of Physics, Federal Research Center KSC
SB RAS, Krasnoyarsk 660036, Russia

3 Siberian Federal University, Krasnoyarsk 660041, Russia

size could be explained by the processes of creation of vortices on the antidot boundaries and their movement towards the sample center, accompanied by energy dissipation.

This paper is organized as follows. The method for calculating the magnetic flux distribution in a superconductor with holes is described in the "Model" section. The "Results" section includes the calculated magnetic flux profiles, epy analysis of the occurrence of secondary peaks, and the dependence of the magnitude of trapped flux on the hole size. The "Discussion" section is devoted to the comparison of simulations with experimental observations.

2 Model

The magnetic flux profiles can be calculated by simulating the vortex lattice interacting with holes and other inhomogeneities (pinning centers) in a superconductor. The calculations were performed for a model layered HTS with holes by means of the continuum-space MC method, with the processes of vortex movement, creation, and annihilation in a layered HTS with holes taken into account [15, 16] (see Appendix 1). In our simulations, samples are magnetized in the following way. An external field of the order of several Tesla is applied, after which a configuration of vortices corresponding to this field is calculated. Then, the external field is removed, and the calculation, during which the vortices exit the sample, takes the same number of MC algorithm steps as it did when the field was nonzero. During this time, the massive avalanche-like relaxation of vortices ceases and the remaining vortices form the trapped magnetic flux.

To calculate the spatial profile of the trapped magnetic flux, we divide the sample into cells of size $\xi < dx < \lambda$, so that there are approximately 100 cells along each side. Here, ξ is the coherence length, λ is the London penetration depth. The magnetic field in the center of each cell is calculated as a sum of the fields generated by all vortices spaced no further than 5λ away (this is the distance beyond which the vortex-vortex interactions can be neglected). The magnetic field of a single vortex equals $B(r) = \frac{\Phi_0}{2\pi\lambda^2} K_0\left(\frac{r}{\lambda}\right)$, where r is the distance from the vortex center to the point at which the field is determined. This procedure is done for an instant vortex configuration at the end of each calculation. Then, the contributions from each vortex are summed over the area corresponding to that of a measuring probe used in experiments. Each point of the calculated profile thus corresponds to the position of the probe center.

The trapped field profiles were calculated for the following parameters: $\xi = 4$ nm, $\lambda = 360$ nm, and $d = 0.27$ nm, which are close to the ones known for HTS (such as Bi-2212, YBCO) at 77 K. Here, d is the thickness of a superconducting layer. Due to certain limitations of CPU speed and memory, the sample size and the external magnetic field in the calculations were limited to values of the order of 10 μm and 0.3 T, respectively.

3 Results

Samples with a regular square lattice of 4, 9, and 16 holes were modeled. Beside the flux trapping on holes, strong ($\alpha = 10$ eV), medium ($\alpha = 3.33$ eV), and weak ($\alpha = 1$ eV) pinning of vortices on nanosized defects is treated. The depth of the potential well near the hole boundary, α_h, is set to 40 eV, which is much higher than α. We use a sample notation that contains information on the number of holes and pinning strength (Table 1). For example, #4 m denotes the sample with 4 holes and medium (m) pinning.

The resulting trapped field profiles for samples #9w, #9 m, and #9 s are presented in Fig. 1. For weak and medium pinning, the secondary peaks of the trapped fields are clearly observed. These peaks correspond to the position of holes. It can be clearly seen that the peaks smear out with increasing pinning strength. As it is expected, the trapped field in the sample center and the trapped flux are higher for the case of stronger pinning.

As it happens in experiments, the size of the measuring probe is crucial for the resulting shape of trapped field profiles. The probe size is simulated by changing the size of the mesh imposed on the sample. Figure 2 shows how the secondary peaks smear out, blend in with the background, and dissolve as the probe size increases.

The trapped flux Φ is expected to vary with the hole size [12]. Figure 3 shows the trapped flux versus the radius of holes R_h for #4w, #4 s, #9w, and #9 s. Φ is almost independent of R_h in the samples with strong pinning (#4 s, #9 s). The cases of weak pinning (samples #4w, #9w) demonstrate an increase in Φ with R_h. A heuristic formula, which is based on the critical state model [17] (see Appendix 2), is suggested to describe the $\Phi(R_h)$ dependence for all cases:

$$
\Phi = \pi\mu_0 j_c R^3 \left[\frac{1}{3} + (k_h - 1)\left(\frac{\rho_h}{R}\right)^2 - \left(k_h - \frac{2}{3}\right)\left(\frac{\rho_h}{R}\right)^3 \right]
\tag{1}
$$

where $\rho_h = A_h N_h R_h$, R is a half-wide of the sample, N_h is the number of holes, and A_h and k_h are positive coefficients, $A_h \leq 1$, $k_h \geq 1$. The coefficient A_h depends on the arrangement

Table 1 Notation of the simulated samples

Pinning strength	4 holes	9 holes	16 holes
Weak $\alpha = 1$ eV	#4w	#9w	#16w
Medium $\alpha = 3.33$ eV	#4 m	#9 m	#16 m
Strong $\alpha = 10$ eV	#4 s	#9 s	#16 s
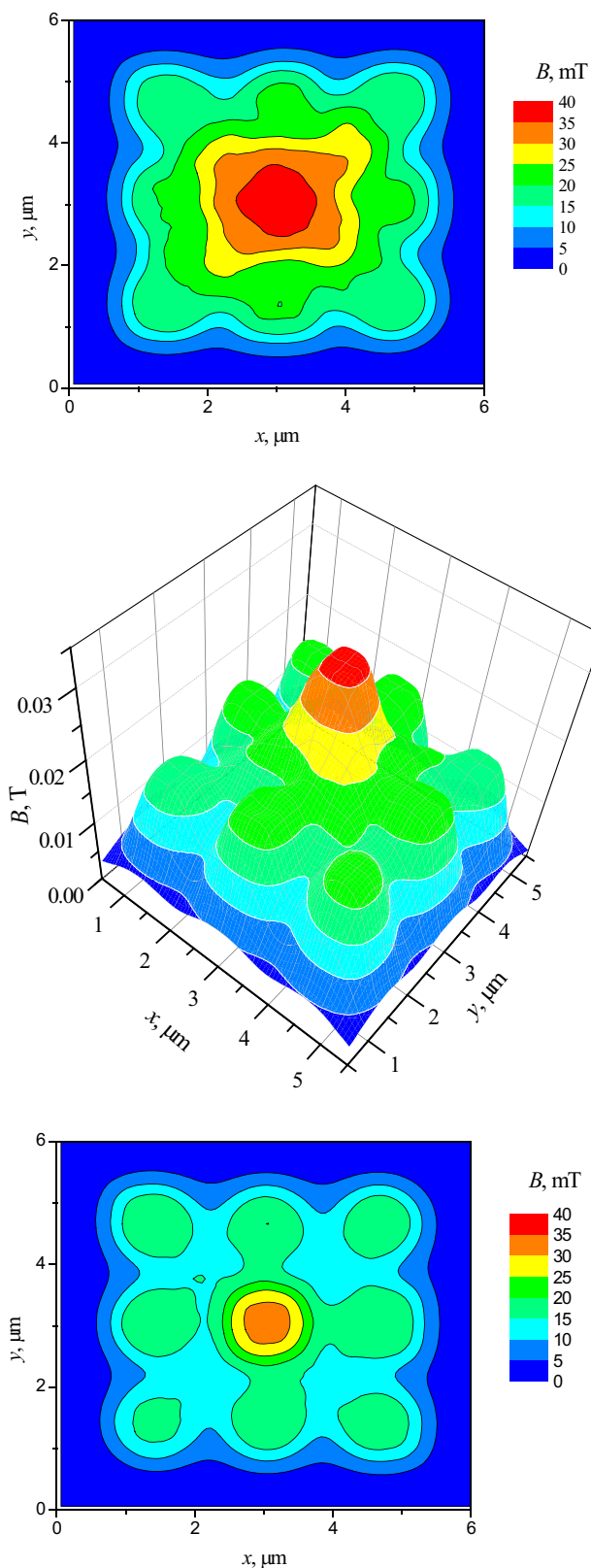
Fig. 1 Trapped magnetic field for #9 s **a**, #9 m (3D graph) **b**, #9w **c**. The hole radius equals 300 nm. The probe size equals the mesh step

of the holes; the coefficient k_h determines the excess trapped flux in the holes. This formula accounts for the competition of the excess flux trapping in the holes [16] and the perturbation of current paths [12]. These competing effects provide the positive and negative slopes on the $\Phi(R_h)$ dependence. The maximum locates at $\rho_h/R = (2k_h-2)/(3k_h-2)$.

The data resulting from the MC calculations are satisfactorily fitted by Eq. (1) with $j_c = 1.1 \cdot 10^{10}$ A m^{-2} for strong pinning (#4 s, #9 s) and $j_c = 3.3 \cdot 10^9$ A m^{-2} for weak pinning (#4w, #9w) (Fig. 3). For each curve, the coefficients $A_h = 0.39$ and $k_h = (2.2 \cdot 10^{10}$ A m$^{-2})/j_c$ are used. The behavior of the fitted $\Phi(R_h)$ dependences shows that it may be possible to optimize the total trapped flux by tuning the sizes, numbers, and positions of holes.

4 Discussion

Let us consider some experimental data on the trapped field in perforated superconductors. Most of experimental investigations of the trapped field in HTS are carried out on macroscopic samples with the typical sizes of about 5–40 mm and applied magnetic fields exceed 1 T [18–21]. Given such conditions, the MC calculations would require large computer resources and take too long. However, there is a qualitative agreement between the experimental data and the obtained computational results for smaller samples.

The trapped field profiles usually have a conical shape for samples with various aspect ratios [22]. The existence of shape distortions and secondary peaks on the trapped field profiles indicates that the sample has sufficiently large defects [23, 24], e.g., holes [25–29] and pores [30, 31]. Such defects trap the magnetic flux quite effectively.

The distortions of trapped field profiles are a typical manifestation of holes [25–29]. However, prominent secondary peaks were rarely observed for perforated samples. In work [25], such peaks occurred at points that coincided with the positions of 1.1-mm holes. Nonetheless, similar samples with smaller holes (with a diameter of 0.7 mm) [25, 27] did not demonstrate any secondary peaks on the trapped field profiles. We suggest that magnetic flux concentrations were not reliably established for small holes in these papers due to the insufficient resolution and/or a relatively large size of the used Hall probes. The disappearance of secondary peaks in the case of large probe sizes (modeled by using coarser meshes in our computations) was demonstrated in the previous section.

A perforated superconductor may be considered as a model of an HTS foam, a peculiar special case of an inhomogeneous superconductor [32, 33]. Numerous pores in the foam act not only as pinning centers, but also as channels

Fig. 2 Trapped magnetic field for #16 m. The hole radius equals 300 nm. The probe size is 0.4 μm **a**, 1 μm **b**, 1.6 μm **c**
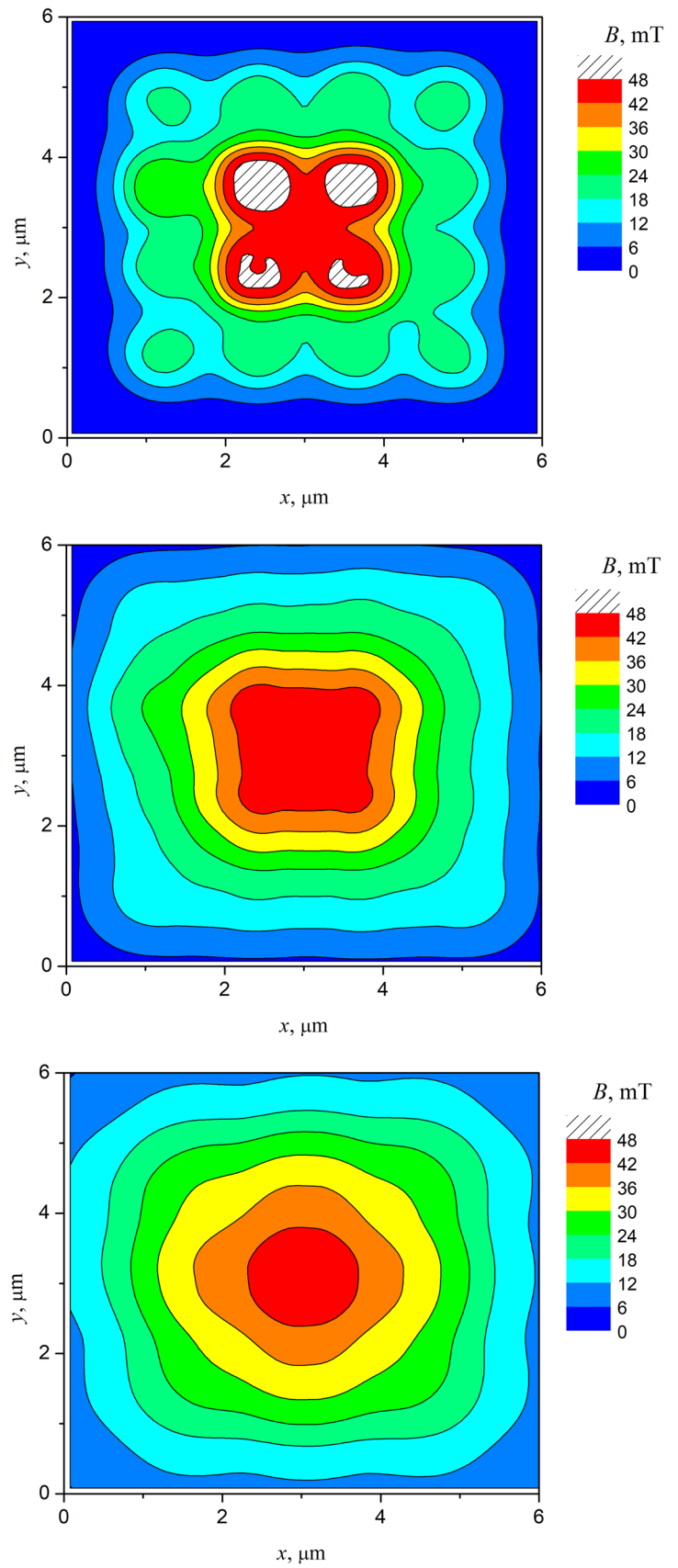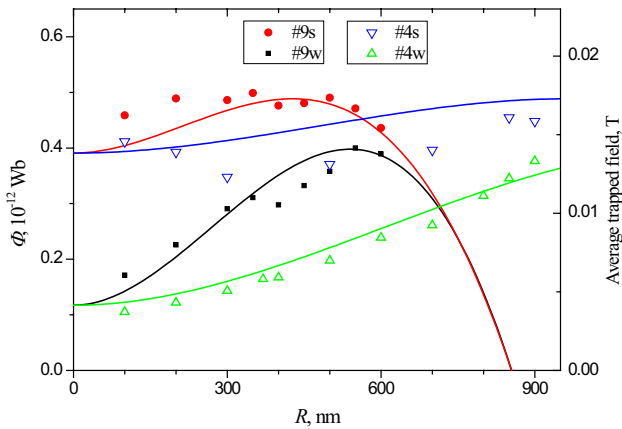
Fig. 3 The trapped flux versus the radius of holes. The points are the results of the MC calculations. The lines are computed by means of Eq. (1)

for the coolant flow, which significantly reduces the cost of cooling. Currently, much attention is paid to the magnetic properties of the foams, such as the flux trapping ability. Apparent secondary peaks on the trapped field profiles were observed for a YBCO foam with 1-mm pores in papers [30, 31]. These secondary peaks are associated with groups of pores, instead of a single pore [30].

Thus, the peculiarities of the trapped field profiles, which are inherent in perforated and porous superconductors, can be reproduced by means of MC calculations in much smaller samples. As our previous computations of the magnetization processes and critical current have shown, the results obtained for micron-sized samples can be extrapolated to samples with the size of a few millimeters.

The state-of-art technologies can produce perforated HTS films with the sizes of a few micrometers [9]. However, it is problematic to measure the trapped field profiles of such films because the Hall probes are of larger sizes. The scanning magnetic microscopy [34], on the other hand, could be interesting to be applied for this task.

The ability to control and adjust the trapped field profiles by varying the number, size, and position of holes or pores in the superconductor pave a new way towards different applications of superconducting trapped field magnets, e.g., in spacecrafts [35].

5 Conclusion

The trapped magnetic flux has been calculated for perforated square plates by means of the Monte Carlo method. Secondary peaks have been found to emerge on the magnetic profiles at points corresponding to the positions of

holes. To provide the excess flux trapping, the energy potential of the holes should be much deeper than that of the ordinary intrinsic pinning centers. Moreover, the probe resolution should be sufficiently high to register the secondary peaks.

The computed dependencies of the trapped flux on the hole radius are fitted by Eq. (1) accounting for the excess flux trapping in the holes and the perturbation of current paths caused by the holes. The trapped flux increases with each added perforation until an optimal density of holes is reached. A further increase in the number of perforations leads to a decrease in the trapped flux. In this case, a choice should be made between the excess trapped flux and the efficiency of cooling due to a better coolant circulation through the system of holes or open pores.

Appendix 1 Monte Carlo Simulations of the Vortex System

During the calculations, the total energy G of the system is minimized. For a system of quasi-two-dimensional vortices (pancakes) in the presence of pinning centers, G has the following form:

$$G = \sum_z \left\{ N_z \varepsilon + \sum_{i<j} U_{\text{in-plane}}(r_{ij}) + \sum_{i,N_p} U_p(r_{ip}) \right.$$
$$\left. + \sum_{i,j} U_{\text{surf}}\left(r_i, r_j^{\text{image}}\right) + \sum_i U_{\text{surf}}^{(\text{Meissner})} \right\}, \quad (A1)$$

$$U_{\text{in-plane}}(r_{ij}) = d \frac{\Phi_0^2}{8\pi^2\lambda^2} K_0\left(\frac{r_{ij}}{\lambda}\right), \quad (A2)$$

$$U_{\text{surf}}\left(r_i r_j^{\text{image}}\right) = -d \frac{\Phi_0^2}{8\pi^2\lambda^2} K_0\left(\frac{\left|r_i - r_j^{(\text{image})}\right|}{\lambda}\right), \quad (A3)$$

where $\varepsilon = \Phi_0^2 d \left[\ln(\lambda/\xi) + 0.52\right]/(4\pi\lambda)^2$ is the self-energy of a vortex, $\Phi_0 = \pi hc/e$ is the magnetic flux quantum, ξ and λ are the coherence length and magnetic penetration depth, N_z is the number of pancakes in the z-plane, r_{ij} and r_{ip} are the absolute values of the position vectors connecting two vortices and a vortex with a pinning center, respectively, d is the thickness of a superconducting layer, and K_0 is the MacDonald function (the modified Bessel function of the second kind). The second term in (A1) describes the pair interaction of vortices inside a superconducting plane, the third one is the interaction of vortices with pinning centers, the fourth is the interaction of a vortex with its reflection with respect to the boundary, and the fifth is the interaction with the Meissner current (the superconductor is in an external magnetic field H).

Let us consider a superconducting sample in the form of a rectangular parallelepiped, the base of which has a size $b \gg \lambda$, placed in a magnetic field perpendicular to the base of the parallelepiped. The superconducting layers are thus also located perpendicular to the magnetic field. Let the base of the parallelepiped coincide with the xy-plane. In the z-direction, we introduce periodic boundary conditions to exclude the effects of demagnetization. In a layered HTS, the vortex lattice is a three-dimensional system, and it is necessary to consider the interaction of pancakes located in the same layer and in neighboring layers for a correct description of the system. However, as most of our calculations show, for a qualitative description of the system, it is acceptable to neglect the inter-plane interactions and consider only one layer as an average response of the entire sample. This is confirmed, in particular, by the coincidence (within the margin of error) of the magnetization curves calculated in the framework of a two-dimensional and three-dimensional model.

The interaction of a vortex with the Meissner current at the boundary is described by an expression of the form [14]

$$U_{\text{surf}}^{\text{(Meissner)}} = d\frac{\Phi_0}{4\pi}H\left(\frac{\cosh\left(\frac{x}{\lambda}\right)}{\cosh\left(\frac{L_x}{2\lambda}\right)} - 1\right), \qquad (A4)$$

where H is the external magnetic field, L_x is the characteristic size that determines the entrance of the vortex into the sample and the interaction of the vortex with the Meissner currents for each point of the surface. Ignoring the rounding near the corners of the square, we can assume that the trajectory of the Meissner currents corresponds to the perimeter of the sample. Then, for each point x, the characteristic size L_x corresponds to the length of the segment passing through x and the sample center from one side of the sample to the other. Using this L_x scale allows us to obtain values of the energy of interaction of vortices with the Meissner currents, qualitatively consistent with experiments. Thus, the force acting on the vortex is always directed towards the sample center.

Since the size of the square-shaped sample is $b \gg \lambda$, the interaction of a vortex with the boundary is introduced as an interaction with the mirror reflections with respect to the two perpendicular boundaries closest to the vortex (Fig. 4). To satisfy the boundary conditions, a third reflection of the same sign as the vortex is introduced. This reflection locates symmetrically relative to the square vertex (Figure 4).
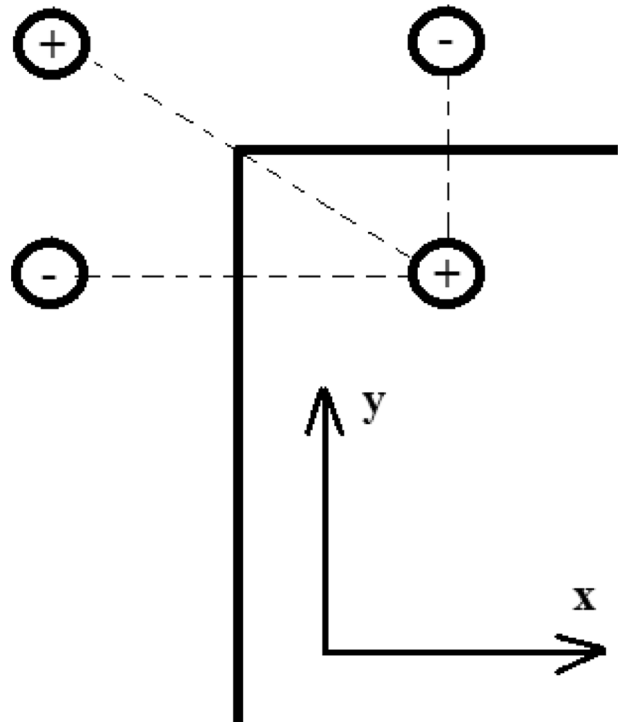

Fig. 4 Interaction of vortex with boundary

The interaction of a vortex with a nanoscale pinning center is described by:

$$U_{\text{p}} = \alpha \frac{1}{1 + r_{ij}/\xi} \exp\left(-\frac{r_{ij}}{2\xi}\right), \qquad (A5)$$

where r_{ij} is the length of the position vector connecting the centers of the vortex and the defect, α is the depth of the potential well of the defect.

The model of a layered HTS with holes was developed in [16]. A submicron hole capable of capturing magnetic flux is introduced into the calculations using the following model approximation. If the radius of the hole is $R_{\text{h}} < \lambda$, then the hole is described as a circular area that vortices cannot enter. This can be modeled by introducing an infinitely large energy inside the hole. Thus, the vortices can be pinned only on the hole edges. If $R_{\text{h}} > \lambda$, vortices can enter the hole. Near the edge of the hole, the interaction energy U_{pn} of the vortex with the defect has the form:

$$U_p = \alpha_h \frac{1}{1 + r_{ij}/\lambda} \exp\left(-\frac{r_{ij}}{2\lambda}\right), \qquad (A6)$$

where r_{ij} is the distance to the edge of the hole, α_h – the depth of the potential well near the edge. This approach simulates the attraction of vortices to the boundary of the hole. We also assume that the vortices trapped by the hole interact in the usual way with the other vortices, with the Meissner current and with their reflection from the sample boundary. This simulates the shielding current around the hole.

Appendix 2 Shrinking of Circulation Area by Holes

Holes can trap excess magnetic flux, but they also perturb the current paths in the sample. These perturbations should decrease the full penetration field H_p.

DLet us consider a simple model sample – a cylinder with a hole along its main axis. The symmetry of the system allows us to work with only one variable r, $r = 0$ on the main axis of the cylinder and $r = R$ on the cylinder's external surface. A positive coefficient k_h is assigned to account for the excess trapped flux in the hole. Perturbations of the current paths caused by the hole and the decrease in H_p are related to the hole radius R_h. The critical state model [17] for such a sample gives $H_p = j_c(R - R_h)$, where j_c is the critical current density (we neglect the field dependence of j_c). Upon magnetizing the sample up to $H >> H_p$ at first and then to $H = 0$, one obtains the trapped field into the sample: $B(r) = \mu_0 j_c(R-r)$ at $R_h \leq r \leq R$ and $B(r) = k_h \mu_0 H_p$ at $0 \leq r < R_h$. The trapped magnetic flux is determined after integration:

$$\Phi = \int_{R_h}^{R} 2\pi r \mu_0 j_c(R - r)dr + \int_0^{R_h} 2\pi r k_h \mu_0 H_p dr$$
$$= \pi \mu_0 j_c R^3 \left[\frac{1}{3} - \left(\frac{R_h}{R}\right)^2 + \frac{2}{3}\left(\frac{R_h}{R}\right)^3 \right. \qquad (B1)$$
$$\left. + k_h \left(\frac{R_h}{R}\right)^2 \left(1 - \frac{R_h}{R}\right)\right].$$

To account for additional holes in the sample, we suggest to replace R_h in (B1) by an effective hole radius $\rho_h = A_h N_h R_h$, where N_h is the number of holes and A_h is the positive coefficient depending on the hole positions. Equation (1) is the result of this approximation.

Data Availability The data that support the findings of this study are available from the corresponding author upon reasonable request.

Declarations

Conflict of Interest The authors declare no competing interests.

References

1. Algarni, R., Almessiere, M.A., Slimani, Y., Hannachi, E., Ben Azzouz, F.: Enhanced critical current density and flux pinning traits with Dy_2O_3 nanoparticles added to $YBa_2Cu_3O_{7-d}$ superconductor. J. Alloys Compd. **852**, 157019 (2021). https://doi.org/10.1016/j.jallcom.2020.157019
2. Pham, A.T., Tran, D.T., Pham, H.H., Nam, N.H., Tai, L.T., Tran, D.H.: Improvement of flux pinning properties in Fe_3O_4 nanoparticle-doped $Bi_{1.6}Pb_{0.4}Sr_2Ca_2Cu_3O_{10+\delta}$ superconductors. Mater. Lett. **298**, 130015 (2021). https://doi.org/10.1016/j.matlet.2021.130015
3. Lepeshev, A.A., Patrin, G.S., Yurkin, G.Y., Vasiliev, A.D., Nemtsev, I.V., Gokhfeld, D.M., Balaev, A.D., Demin, V.G., Bachurina, E.P., Karpov, I.V., Ushakov, A.V., Fedorov, L.Y., Irtyugo, L.A., Petrov, M.I.: Magnetic properties and critical current of superconducting nanocomposites (1–x)YBa2Cu3O7−δ + xCuO. J. Supercond. Nov. Magn. **31**, 3841–3845 (2018). https://doi.org/10.1007/s10948-018-4676-x
4. Fan, X.J., Sun, X.F., Zhang, J., Zhao, X., Li, X.G.: Temperature dependence of vortex pinning in re-doped $HgBa_2Ca_2Cu_{2.9}Re_{0.1}O_y$. Physica C. **341**, 1161–1162 (2000). https://doi.org/10.1016/S0921-4534(00)00838-8
5. Haberkorn, N., Suárez, S., Bud'ko, S.L., Canfield, P.C.: Strong pinning and slow flux creep relaxation in Co-doped $CaFe_2As_2$ single crystals. Solid State Commun. **318,** 113963 (2020). https://doi.org/10.1016/j.ssc.2020.113963
6. Petrov, M.I., Gokhfeld, Y.S., Balaev, D.A., Popkov, S.I., Dubrovskiy, A.A., Gokhfeld, D.M., Shaykhutdinov, K.A.: Pinning enhancement by heterovalent substitution in $Y_{1-x}RE_xBa_2Cu_3O_{7-\delta}$. Supercond. Sci. Technol. **21**, (2008). https://doi.org/10.1088/0953-2048/21/8/085015
7. Zehetmayer, M.: How the vortex lattice of a superconductor becomes disordered: a study by scanning tunneling spectroscopy. Sci. Rep. **5**, 9244 (2015). https://doi.org/10.1038/srep09244
8. Haberkorn, N., Suárez, S., Lee, J.H., Moon, S.H., Lee, H.: In-field dependences of the critical current density Jc in $GdBa_2Cu_3O_{7-d}$ coated conductors produced by Zr irradiation and post-annealing at low temperatures. Solid State Commun. **289**, 51–55 (2019). https://doi.org/10.1016/j.ssc.2018.12.008
9. Pokrovskii, S.V., Mavritskii, O.B., Egorov, A.N., Mineev, N.A., Timofeev, A.A., Rudnev, I.A.: Influence of ultrashort laser drilling on magnetic and transport characteristics of HTS tapes. Supercond. Sci. Technol. **32**, 075008 (2019). https://doi.org/10.1088/1361-6668/ab14a3
10. Wu, T.C., Cao, R., Yang, T.J., Horng, L., Wu, J.C., Koláček, J.: Rectified vortex motion in an Nb film with a spacing-graded array of holes. Solid State Commun. **150**, 280–284 (2010). https://doi.org/10.1016/j.ssc.2009.11.006
11. Huang, K.Y., Hlásek, T., Namburi, D.K., Dennis, A.R., Shi, Y., Ainslie, M.D., Congreve, J.V.J., Plecháček, V., Plecháček, J., Cardwell, D.A., Durrell, J.H.: Improved trapped field performance of single grain Y-Ba-Cu-O bulk superconductors containing artificial holes. J. Am. Ceram. Soc. **104**, 18017 (2021). https://doi.org/10.1111/jace.18017
12. Lousberg, G.P., Ausloos, M., Vanderbemden, P., Vanderheyden, B.: Bulk high-Tc superconductors with drilled holes: how to arrange the holes to maximize the trapped magnetic flux? Supercond. Sci.

Technol. **21**, 025010 (2008). https://doi.org/10.1088/0953-2048/21/02/025010

13. Lousberg, G.P., Ausloos, M., Geuzaine, C., Dular, P., Vanderbemden, P., Vanderheyden, B.: Numerical simulation of the magnetization of high-temperature superconductors: a 3D finite element method using a single time-step iteration. Supercond. Sci. Technol. **22**, 055005 (2009). https://doi.org/10.1088/0953-2048/22/5/055005

14. Kashurnikov, V.A., Rudnev, I.A., Zyubin, M.V.: Magnetization of two-dimensional superconductors with defects. J. Exp. Theor. Phys. **94**, 377–386 (2002). https://doi.org/10.1134/1.1458488

15. Moroz, A.N., Maksimova, A.N., Kashurnikov, V.A., Rudnev, I.A.: Influence of antidots on transport characteristics of HTSC. IEEE Trans. Appl. Supercond. **28**, (2018). https://doi.org/10.1109/TASC.2018.2813372

16. Maksimova, A.N., Kashurnikov, V.A., Moroz, A.N., Rudnev, I.A.: Mechanism of the generation of the critical current in high-temperature superconductors with through microdefects. Phys. Solid State. **63**, 64–67 (2021). https://doi.org/10.1134/S1063783421010145

17. Bean, C.P.: Magnetization of high-field superconductors. Rev. Mod. Phys. **36**, 31–39 (1964). https://doi.org/10.1103/RevModPhys.36.31

18. Bartolomé, E., Granados, X., Puig, T., Obradors, X., Reddy, E.S., Schmitz, G.J.: Critical state in superconducting single-crystalline $YBa_2Cu_3O_7$ foams: Local versus long-range currents. Phys. Rev. B - Condens. Matter Mater. Phys. **70**, 144514 (2004). https://doi.org/10.1103/PhysRevB.70.144514

19. Granados, X., Sena, S., Bartolomé, E., Palau, A., Puig, T., Obradors, X., Carrera, M., Amorós, J., Claus, H.: Characterization of superconducting rings using an in-field hall probe magnetic mapping system. IEEE Trans. Appl. Supercond. 3667–3670 (2003)

20. Bernstein, P., Noudem, J., Dupont, L.: Critical current density and current distribution in field cooled superconducting disks. Supercond. Sci. Technol. **29**, 075007 (2016). https://doi.org/10.1088/0953-2048/29/7/075007

21. Shi, Y., Dennis, A.R., Huang, K., Zhou, D., Durrell, J.H., Cardwell, D.A.: Advantages of multi-seeded (RE)-Ba-Cu-O superconductors for magnetic levitation applications. Supercond. Sci. Technol. **31**, 095008 (2018). https://doi.org/10.1088/1361-6668/aad4f1

22. Shi, Y., Dennis, A.R., Durrell, J.H., Cardwell, D.A.: The effect of size and aspect ratio on the trapped field properties of single grain. Y-Ba-Cu-O bulk superconductors. Supercond. Sci. Technol. **32**, 025005 (2019). https://doi.org/10.1088/1361-6668/aaf2ea

23. Eisterer, M., Haindl, S., Zehetmayer, M., Gonzalez-Arrabal, R., Weber, H.W., Litzkendorf, D., Zeisberger, M., Habisreuther, T., Gawalek, W., Shlyk, L., Krabbes, G.: Limitations for the trapped field in large grain YBCO superconductors. Supercond. Sci. Technol. **19**, 530–536 (2006). https://doi.org/10.1088/0953-2048/19/7/S21

24. Ainslie, M.D., Fujishiro, H., Ujiie, T., Zou, J., Dennis, A.R., Shi, Y.H., Cardwell, D.A.: Modelling and comparison of trapped fields in (RE)BCO bulk superconductors for activation using pulsed field magnetization. Supercond. Sci. Technol. **27**, 9 (2014). https://doi.org/10.1088/0953-2048/27/6/065008

25. Haindl, S., Hengstberger, F., Weber, H.W., Meslin, S., Noudem, J., Chaud, X.: Hall probe mapping of melt processed superconductors with artificial holes. Supercond. Sci. Technol. **19**, 108–115 (2006). https://doi.org/10.1088/0953-2048/19/1/018

26. Noudem, J.G., Meslin, S., Horvath, D., Harnois, C., Chateigner, D., Ouladdiaf, B., Eve, S., Gomina, M., Chaud, X., Murakami, M.: Infiltration and top seed growth-textured YBCO bulks with multiple holes. J. Am. Ceram. Soc. **90**, 2784–2790 (2007). https://doi.org/10.1111/j.1551-2916.2007.01841.x

27. Jang, G., Lee, M., Han, S., Kim, C., Han, Y., Park, B.: Trapped field analysis of a high temperature superconducting bulk with artificial holes. J. Magn. **16**, 181–185 (2011). https://doi.org/10.4283/JMAG.2011.16.2.181

28. Yokoyama, K., Igarashi, R., Togasaki, R., Oka, T.: Pulsed field magnetization characteristics of a holed superconducting bulk magnet. Physica C. **518**, 117–121 (2015). https://doi.org/10.1016/j.physc.2015.06.008

29. Dias, D.H.N., Sotelo, G.G., Moysés, L.A., Telles, L.G.T., Bernstein, P., Kenfaui, D., Aburas, M., Chaud, X., Noudem, J.G.: Application of textured YBCO bulks with artificial holes for superconducting magnetic bearing. Supercond. Sci. Technol. **28**, 075005 (2015). https://doi.org/10.1088/0953-2048/28/7/075005

30. Koblischka, M.R., Naik, S.P.K., Koblischka-Veneva, A., Murakami, M., Gokhfeld, D., Reddy, E.S., Schmitz, G.J.: Superconducting YBCO foams as trapped field magnets. Materials. **16**, (2019). https://doi.org/10.3390/ma12060853

31. Koblischka, M.R., Pavan Kumar Naik, S., Koblischka-Veneva, A., Gokhfeld, D., Murakami, M.: Flux creep after field trapping in YBa2Cu3Ox foams. Supercond. Sci. Technol. **33**, 044008 (2020). https://doi.org/10.1088/1361-6668/ab72c3

32. Gokhfeld, D.M., Koblischka, M.R., Koblischka-Veneva, A.: Highly porous superconductors: synthesis, research, and prospects. Phys. Met. Metallogr. **121**, 936–948 (2020). https://doi.org/10.1134/S0031918X20100051

33. Noudem, J.G.: Development of shaping textured YBaCuO superconductors. J. Supercond. Nov. Magn. **24**, 105–110 (2011). https://doi.org/10.1007/s10948-010-0905-7

34. Araujo, J.F.D.F., Reis, A.L.A., Correa, A.A.P., Yokoyama, E., Oliveira, V.C., Mendoza, L.A.F., Pacheco, M.A.C., Luz-Lima, C., Santos, A.F., Osorio G., F.G., Brito, G.E., Araujo, W.W.R., Tahir, Bruno, A.C., Del Rosso, T.: Scanning magnetic microscope using a gradiometric configuration for characterization of rock samples. Materials. **12**, 4154 (2019). https://doi.org/10.3390/ma12244154

35. Yang, W., Liao, D., Ji, Y., Yao, L.: Effects of magnetization conditions on dynamic characteristics of spacecrafts with superconducting flux pinning docking interfaces. J. Appl. Phys. **124**, 213901 (2018). https://doi.org/10.1063/1.5047073